JOURNAL OF APPLIED PHYSICS 110, 073518 (2011)

High-precision characterization of textured a-Si:H/SnO_2:F structures by spectroscopic ellipsometry

Masataka Akagawa and Hiroyuki Fujiwara[a)]
Center of Innovative Photovoltaic Systems (CIPS), Gifu University, 1-1 Yanagido, Gifu 501-1193, Japan

(Received 12 July 2011; accepted 19 August 2011; published online 11 October 2011)

Spectroscopic ellipsometry (SE) has been applied for the characterization of hydrogenated amorphous silicon (a-Si:H) layers formed on SnO_2:F textured structures in an attempt to establish the structural characterization method for a-Si:H solar cells. In particular, an optical model that allows the complete evaluation of microscopically non-uniform a-Si:H/SnO_2:F textured structures has been developed for the SE analysis. In order to express the complicated optical response in the textured structures, the optical model incorporates (i) the surface roughness and interface layers calculated using an effective-medium-approximation multilayer model and (ii) the a-Si:H/SnO_2:F structure divided into two regions with different thicknesses. Using this optical model, SE spectra obtained experimentally from the a-Si:H/SnO_2:F textured structure can be reproduced almost perfectly. The a-Si:H/SnO_2:F structure deduced from the SE analysis shows remarkable agreement with that observed from transmission electron microscopy. Moreover, a variety of a-Si:H layers with different thicknesses are expressed from the identical optical model. The SE analysis method developed in this study can be utilized further to perform high-precision and non-destructive characterization of various a-Si:H layers incorporated in large-area a-Si:H modules. © *2011 American Institute of Physics*. [doi:10.1063/1.3646521]

I. INTRODUCTION

In large-area solar cell modules of hydrogenated amorphous silicon (a-Si:H),[1,2] the structural uniformity of the various component layers is critical in achieving high module efficiencies. In particular, the a-Si:H module consists of a-Si:H *p-i-n* cells having a striped shape, and these elementary cells are integrated using a laser scribing technique.[1,2] In a-Si:H modules, all the a-Si:H elementary cells are connected electrically in series, and the total module current is determined by the elementary cell that shows the lowest current.[3] Accordingly, the total output power in the modules is affected directly by the structural non-uniformity, particularly in a-Si:H layers. In general, the number of elementary cells in an a-Si:H module exceeds 100, and the module power is maximized when all these elementary cells have an identical current. In a-Si:H/μc-Si:H tandem modules, each elementary cell is further composed of a-Si:H-based *p-i-n* and μc-Si:H *p-i-n* unit cells,[1,2] and controlling the structural uniformity becomes even more challenging.

For the characterization of such structural non-uniformities in large-area modules, spectroscopic ellipsometry (SE) is an ideal tool, because SE is a non-destructive technique and enables us to perform high-precision characterization of various film structures and film properties with high speed.[4] So far, the SE characterization of SnO_2:F (Ref. 5) and a-Si:H/SnO_2:F (Ref. 6) textured structures has been reported. Fortunately, in such SE analyses, the effect of light scattering on textured surfaces can be neglected, as the scattered light waves have different reflection angles and the contribution of the scattered light is quite small in actual ellipsometry measurements. Thus, even for textured structures, SE analysis can be carried out relatively easily using a conventional optical model.[5,6] However, the SnO_2:F textured structure used in a-Si:H solar cells is microscopically quite inhomogeneous,[7,8] because the SnO_2:F texture is generated by the crystallographic SnO_2 grain growth.[8] Accordingly, proper SE analysis methods should be established to perform high-precision analyses of the non-uniform textured structures adopted in a-Si:H solar cells.

In this study, we have characterized a-Si:H layers formed on textured SnO_2:F transparent conductive oxide (TCO) layers by applying SE. For the characterization of the textured a-Si:H/SnO_2:F structure, an optical model that can be applied to the SE analysis has been developed. As a result, we have demonstrated that the microscopically inhomogeneous a-Si:H/SnO_2:F textured structure can be determined quite accurately by SE, and the textured structure deduced from our SE analysis agrees with the actual structure almost perfectly.

II. EXPERIMENT

To develop the SE analysis method for a-Si:H/SnO_2:F textured structures, we prepared a-Si:H layers on textured SnO_2:F-coated glass (Asahi-U) substrates using plasma-enhanced chemical vapor deposition. A series of a-Si:H layers with different thicknesses (130 to 500 nm) were fabricated using a substrate temperature of 180 °C, a SiH_4 flow rate of 5 SCCM (SCCM denotes cubic centimeters per minute at standard temperature and pressure), a rf power of 13 mW/cm^2, and a pressure of 50 mTorr.[9] These deposition conditions yield a relatively slow deposition rate of 0.4 Å/s.

Figure 1 shows scanning electron microscope (SEM) images obtained from (a) the textured SnO_2:F (Asahi-U)

[a)]Author to whom correspondence should be addressed. Electronic mail: fujiwara@gifu-u.ac.jp.

 © 2011 American Institute of Physics

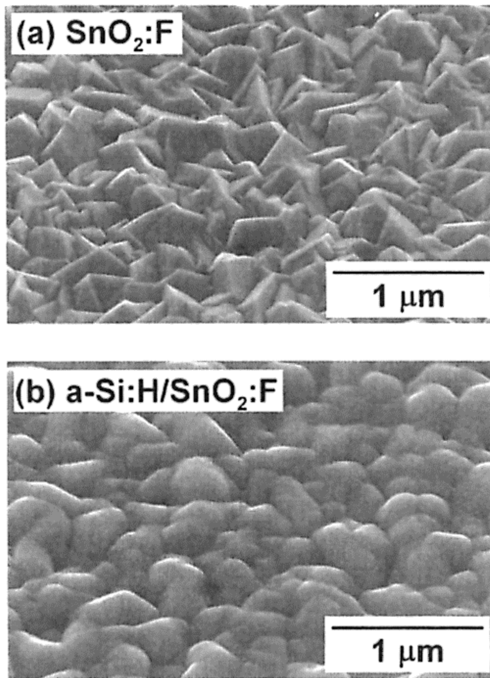

FIG. 1. SEM images of (a) the textured SnO_2:F layer on a glass substrate (Asahi-U) and (b) the a-Si:H layer (~260 nm) deposited on the textured SnO_2:F layer.

substrate and (b) the a-Si:H layer (~260 nm) deposited on the textured SnO_2:F substrate. As shown in Fig. 1, the textured structures have sub-micron dimensions and are microscopically quite inhomogeneous. It should be emphasized that the surface morphology changes drastically after the a-Si:H deposition. In particular, the sharp crystallographic feature of the SnO_2:F texture is lost completely after isotropic a-Si:H deposition on the SnO_2:F texture, as will be shown in Fig. 11.

The (ψ, Δ) ellipsometry spectra of the samples were measured *ex situ* using a rotating-analyzer ellipsometry instrument with a compensator (J. A. Woollam, VASE). The SE measurements were performed at room temperature using an incidence angle of 55°, which corresponds to the Brewster angle of glass substrates. The spot size of the SE light probe was 1 mm, and the SE spectra were rather independent of the measurement spot size.

III. SE ANALYSIS

A. Optical model for textured structures

In a conventional SE analysis, an optical model defined by optical constants (or dielectric function) and layer thickness is required.[4] For the characterization of the textured SnO_2:F substrate, an optical model consisting of an ambient/(surface roughness layer)/(SnO_2:F bulk layer)/(SnO_2 transparent layer)/(glass substrate) structure can be used. The SnO_2 transparent layer in the above-described model represents the SnO_2 layer with a low carrier concentration without significant free-carrier absorption. The optical properties of the surface roughness layer were modeled as a 50/50 vol.% mixture of the SnO_2:F bulk layer and voids using the Bruggeman effective-medium approximation (EMA).[4] A similar

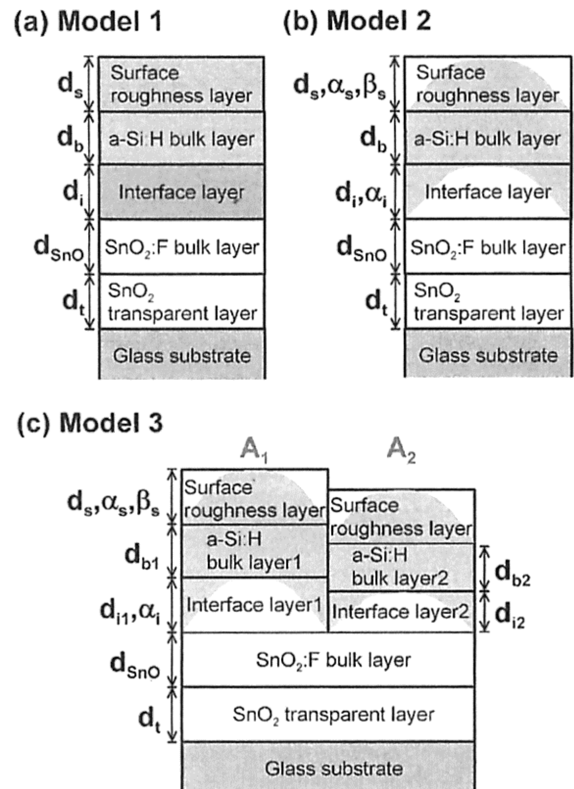

FIG. 2. (Color online) Optical models used for the SE analyses of the a-Si:H/SnO_2:F textured structures: (a) conventional model (model 1), (b) EMA multilayer model (model 2), and (c) surface area model combined with EMA multilayer model (model 3).

optical model has been reported for the SE analysis of textured SnO_2:F layers.[5]

Figure 2 shows three different optical models constructed in this study to analyze the a-Si:H/SnO_2:F textured structures: (a) a conventional model (model 1), (b) an EMA multilayer model (model 2), and (c) a surface area model combined with an EMA multilayer model (model 3). In model 1, the surface roughness and interface layers are assumed to be single layers having uniform optical constants, and the optical constants of the surface roughness and interface layers are calculated from 50/50 vol.% mixtures of the a-Si:H/void and a-Si:H/SnO_2:F components, respectively, by applying EMA. The structure in this model is determined by the layer thicknesses of the surface roughness layer (d_s), the a-Si:H bulk layer (d_b), the interface layer (d_i), the SnO_2:F bulk layer (d_{SnO}), and the SnO_2 transparent layer (d_t).

In order to express the optical response in the a-Si:H surface roughness and a-Si:H/SnO_2:F interface regions accurately, we have developed the EMA multilayer model in this study. In model 2, the optical response of the surface roughness and interface layers is represented by this EMA multilayer model. Figure 3 shows the schematic structure of the EMA multilayer model. In this model, a two-phase mixture is assumed in a cylindrical geometry with a radius of $r = 1$. The variation of the two-phase composite has been modeled by $d(r) = d_0(1 - r^{\alpha})$, where d_0 is the thickness of the surface roughness and interface layers at $r = 0$, and α shows the curvature of $d(r)$ in the cross-section of the cylinder. When $\alpha = 1$, the variation of the two-phase composite at the

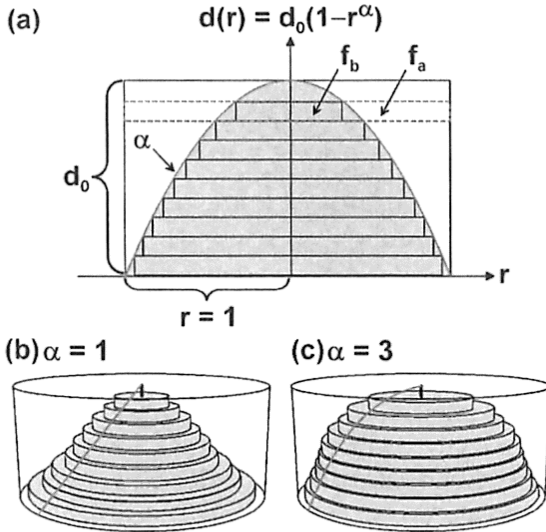

FIG. 3. (Color online) EMA multilayer model used for the calculation of the surface roughness and interface layers in model 2 and model 3: (a) The calculation method of the EMA multilayer model and the variation of the two-phase composite when (b) $\alpha = 1$ and (c) $\alpha = 3$. In (a), r, d_0, and α denote the radius, the thickness of the layer, and the curvature, and f_a and f_b show the volume fractions of phases a and b ($f_b = 1 - f_a$), respectively.

cylinder cross-section becomes linear, whereas the variation shows a round shape at $\alpha > 1$, as confirmed from Figs. 3(b) and 3(c).

In the EMA multilayer model, a total of 10 layers are assumed, and the volume fractions of the two-phase mixture (f_a and f_b) in each layer are obtained using $r(d) = (1 - d/d_0)^{1/\alpha}$, which can be derived directly from $d = d_0(1 - r^\alpha)$. The volume of the cylinder plate for the *j*th layer at the thickness d_j is expressed simply by $V(d_j) = \pi r(d_j)^2(d_0/m)$, where m is the total number of layers used in the analysis (m = 10 in this study). In our model, f_a and f_b are calculated from the volume ratio defined by

$$f_a(d_j) = \frac{V(0) - V(d_j)}{V(0)}\beta, \tag{1}$$

$$f_b(d_j) = 1 - f_a(d_j), \tag{2}$$

where V(0) shows the total volume of the cylinder with a thickness of d_0/m. In Eq. (1), we have introduced an additional parameter, β, which represents the volume fraction of f_a in the top layer. In particular, when $\beta = 1$, the volume fractions in the top layer become $f_a = 1$ and $f_b = 0$, because $r(d_0) = V(d_0) = 0$. Thus, through the introduction of the parameter β, the structural variation can be controlled more precisely.

Once the volume fractions of f_a and f_b are known, the optical properties of each layer are calculated using EMA. The optical response of the whole structure in Fig. 3(a) can then be determined by considering the conventional interference effect in the EMA multilayer. In model 2, shown in Fig. 2(b), the calculation of the surface roughness layer was performed assuming $f_a = f_{void}$ and $f_b = f_{a\text{-}Si:H}$ in Fig. 3(a), where f_{void} and $f_{a\text{-}Si:H}$ denote the volume fractions of void and a-Si:H components, respectively. For the a-Si:H/SnO_2:F interface layer in model 2, we assumed $f_a = f_{a\text{-}Si:H}$ and $f_b = f_{SnO}$, where f_{SnO} is the volume fraction of the SnO_2:F layer. In the case of the surface roughness layer in Fig. 2(b), we employed three parameters, d_s, α_s, and β_s, that correspond to d_0, α, and β described above. For the interface layer, however, we employed two parameters, d_i and α_i, corresponding to d_0 and α assuming $\beta = 1$. In this particular case, the top layer in the multilayer becomes $f_a = f_{a\text{-}Si:H} = 1$, and the contribution of this layer is incorporated into the a-Si:H bulk layer.

For a detailed analysis of the complicated a-Si:H/SnO_2:F textured structures, we have further developed model 3, shown in Fig. 2(c). In this model, in order to express the structural inhomogeneity of the a-Si:H on the textured SnO_2:F substrate, the multilayer structure is divided into two regions having different thicknesses. The amplitude reflection coefficient of the optical model is calculated simply by $r_{total} = A_1 r_1 + A_2 r_2$, where A_k and r_k show the surface area fractions ($A_1 + A_2 = 1$) and amplitude reflection coefficients of the two regions, respectively. By calculating r_{total} for p- and s-polarizations, (ψ, Δ) can be obtained as $\tan\psi \exp(i\Delta) = r_{total,p}/r_{total,s}$. The above-described surface area model has already been utilized in the SE analysis of island film structures[10] and pattern-etched samples.[11,12]

In the analysis of model 3, the EMA multilayer model has also been applied. For the surface roughness layer of the two regions in Fig. 2(c), we used the same parameters (d_s, α_s, β_s) to reduce the number of free parameters. In the case of the interface layers, on the other hand, different layer thicknesses (d_{i1}, d_{i2}) with the same α_i ($\beta_i = 1$) were used for the two regions. In the SE analysis of model 3, the bulk layer thicknesses of the a-Si:H layers (d_{b1}, d_{b2}) and the SnO_2:F layer (d_{SnO}) were varied as analysis parameters, and we assumed $A_1 = A_2 = 0.5$.

In the SE analyses of Fig. 2, d_t was estimated in advance from the characterization of the textured SnO_2:F samples, although d_t can still be used as a free parameter. As a result, the total number of analysis parameters in Fig. 2 becomes four (model 1), seven (model 2), or nine (model 3). It should be emphasized that the effect of light scattering on textured surfaces has been neglected completely in our analysis, and the calculation of all the optical models shown in Fig. 2 has been performed using conventional Fresnel equations, assuming that no scattered light is detected in the SE measurements.

From the SE analysis, we further deduced the effective thickness of the a-Si:H layer (d_{eff}) described below. In the case of model 1 in Fig. 2(a), the effective thickness is defined by $d_{eff} = d_b + 0.5(d_s + d_i)$, where the coefficient of 0.5 indicates $f_{a\text{-}Si:H}$ in the surface roughness and interface layers. Thus, d_{eff} represents the a-Si:H thickness when the layer structure is perfectly flat. In the case of model 2, d_{eff} is obtained from

$$d_{eff} = d_b + \sum_{j=1}^{10} d_{s,j} f_{a\text{-}Si:H}(d_{s,j}) + \sum_{j=1}^{9} d_{i,j} f_{a\text{-}Si:H}(d_{i,j}), \tag{3}$$

where $d_{s,j}$ and $d_{i,j}$ denote the thickness of the *j*th layer for the surface roughness and interface layers, respectively. For the interface layer, there are only nine layers, because the contribution of the top layer has been incorporated into d_b, as mentioned earlier. The d_{eff} of model 3 can also be calculated in a similar way and is given by $d_{eff} = A_1 d_{eff,A1} + A_2 d_{eff,A2}$.

Here, $d_{eff,A1}$ and $d_{eff,A2}$ show the d_{eff} for the A_1 and A_2 regions in Fig. 2(c) and are calculated using Eq. (3).

In the fitting analysis of the SE spectra, we employed a fitting error function expressed by

$$\chi^2 = \frac{1}{2N-M}\sum_{j=1}^{N}\left\{\left[\frac{\psi_{ex}(E_j)-\psi_{cal}(E_j)}{\delta\psi(E_j)}\right]^2 + \left[\frac{1}{4}\left(\frac{\Delta_{ex}(E_j)-\Delta_{cal}(E_j)}{\delta\Delta(E_j)}\right)\right]^2\right\}, \tag{4}$$

where N and M show the number of measured (ψ, Δ) pairs for photon energies and the number of analytical parameters, respectively. The subscripts "ex" and "cal" in Eq. (4) denote experimental and calculated values at the photon energy of E_j, respectively, and ($\delta\psi$, $\delta\Delta$) denotes measurement errors in (ψ, Δ). In Eq. (4), the fitting error is estimated from the weighted function of the measurement errors, and such a fitting error is generally referred to as the biased estimator χ^2 (Refs. 13 and 14). A similar equation has been employed in previous SE analyses.[15] In our fitting function, however, the fitting error for Δ is divided by four, because the measurement range for Δ is $0° \leq \Delta \leq 360°$ (or $-180° \leq \Delta \leq 180°$) and is four times larger than that for ψ ($0° \leq \psi \leq 90°$). If the SE analysis is performed without the coefficient of 1/4 in Eq. (4), the Δ spectrum is fitted predominantly, compared with the ψ spectrum, as the variation in Δ is much larger (see Figs. 5 and 7). We confirmed that the coefficient of 1/4 for Δ has only small effects on the confidence limits of the analytical parameters calculated from a standard procedure.[15]

B. Dielectric functions of a-Si:H and SnO_2 layers

For the SE analysis, dielectric functions (or optical constants) of each component layer are required.[4] For the glass substrate, a fixed refractive index of n = 1.46 was used, because the optical properties of the glass employed in the Asahi-U substrate were not clear. Nevertheless, the SE results are rather insensitive to the refractive index of the glass substrate due to the weak light reflection at the SnO_2–glass interface, and refractive indices ranging from n = 1.46 to 1.52 give almost identical results. In order to simplify the SE analysis, the a-Si:H dielectric function was obtained from an a-Si:H layer deposited on a flat crystalline silicon (c-Si) substrate covered with native oxide.[9] The determined dielectric function was then used for the analysis of the a-Si:H/SnO_2:F textured structures. In this analysis, therefore, we assumed that the a-Si:H dielectric function is independent of the substrate morphology. For the SE analysis, we parameterized the a-Si:H dielectric function by applying the Tauc-Lorentz (TL) model.[16] In this model, the dielectric function is described by five independent parameters; namely, an amplitude parameter (A_{TL}), a broadening parameter (C), the bandgap (E_g), the peak position of an ε_2 peak (E_0), and an ε_1 value at high energies {$\varepsilon_1(\infty)$}.[16] The TL parameters for our a-Si:H layer are $A_{TL} = 211.90$ eV, $C = 2.33$ eV, $E_g = 1.688$ eV, $E_0 = 3.656$ eV, and $\varepsilon_1(\infty) = 0.440$.[9]

To express the free carrier absorption in various TCO layers, the Drude model has been employed.[5,17] In the Drude model, the free carrier absorption is described completely by using two parameters: A_D and Γ. For the interband transition that occurs above the bandgap of TCO, the TL model can also be applied.[5,17] By combining these models, the dielectric function of the TCO layers is expressed as $\varepsilon(E) = \varepsilon_{TL}(E) + \varepsilon_{Drude}(E)$, where $\varepsilon_{TL}(E)$ and $\varepsilon_{Drude}(E) = -A_D/(E^2 - i\Gamma E)$ indicate the dielectric functions calculated by the TL and Drude models, respectively. As a result, the dielectric function of the SnO_2 layers can be parameterized using a total of seven parameters {A_{TL}, C, E_g, E_0, $\varepsilon_1(\infty)$, A_D, Γ}.[5,17] We determined these parameter values from the measurement of the textured SnO_2:F substrate prior to the a-Si:H deposition, and the optical parameters estimated from this analysis were used as fixed parameters in the SE analysis.

Figure 4 summarizes the dielectric functions of (a) the a-Si:H layer and (b) the SnO_2:F bulk and SnO_2 transparent layers extracted from a textured SnO_2:F substrate. The parameter values for the SnO_2:F layer are $A_{TL} = 379$ eV, $C = 12$ eV, $E_g = 5.5$ eV, $E_0 = 7.0$ eV, $\varepsilon_1(\infty) = 1$, $A_D = 1.22$ eV, and $\Gamma = 0.18$ eV, whereas those for the SnO_2 transparent layer are $A_{TL} = 114$ eV, $C = 12$ eV, $E_g = 3.0$ eV, $E_0 = 9.0$ eV, $\varepsilon_1(\infty) = 1$, $A_D = 1.27$ eV, and $\Gamma = 0.02$ eV. In the SE analysis of the SnO_2:F textured substrates, the fitting quality deteriorates at $E > 3.0$ eV. In Fig. 4(b), therefore, the dielectric functions up to 3 eV are shown. It should be noted that the optical properties of the SnO_2 layers at $E > 3$ eV can be neglected in the analysis of the a-Si:H/SnO_2:F structures, because the optical response in this region is predominantly determined by the a-Si:H top layer, as will be discussed in Sec. IV.

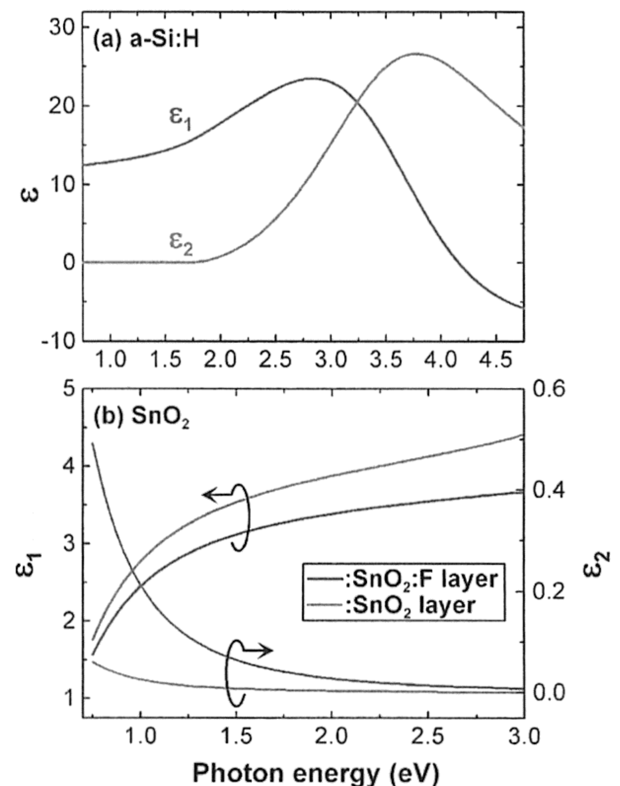

FIG. 4. (Color online) Dielectric functions of (a) the a-Si:H layer and (b) the SnO_2:F bulk layer (lower curve for ε_1 and upper curve for ε_2) and SnO_2 transparent layer (upper curve for ε_1 and lower curve for ε_2) employed for the SE analyses shown in Fig. 2.

IV. RESULTS AND DISCUSSION

A. SE analyses using different optical models

In order to establish the SE analysis method for a-Si:H/SnO_2:F textured structures, we have performed the fitting analysis of ellipsometry (ψ, Δ) spectra using the different optical models described in Sec. III A. Figure 5 shows the SE spectra obtained from the a-Si:H/SnO_2:F textured structure (open circles). In Fig. 5, the d_{eff} of the a-Si:H layer obtained from model 3 is 392 ± 13 nm. The solid lines in Fig. 5 represent the fitting results calculated from (a) model 1, (b) model 2, and (c) model 3 in Fig. 2, and the χ^2 values obtained from each model are also shown in Fig. 5. In these analyses, a fixed value of $d_t = 145$ nm was employed.

In the case of model 1, the overall fitting is quite poor and the χ^2 value is quite high ($\chi^2 = 305.5$), although the fitting improves in a low energy region (E < 1.5 eV). At high energies (E > 3.0 eV), the (ψ, Δ) spectra are determined by the near-surface optical response, because the absorption coefficients in the a-Si:H layer are quite large in this region and the resulting penetration depth of light becomes quite small. Thus, the large deviation from the experimental spectra at E > 3.0 eV in model 1 indicates that the surface roughness layer cannot be represented by a single layer with uniform optical constants.

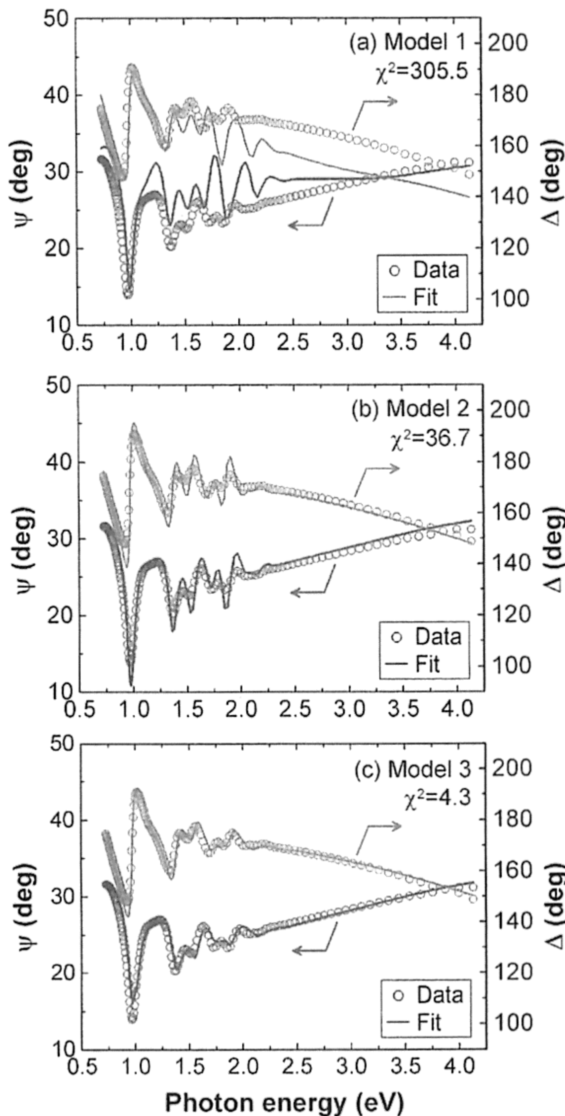

FIG. 5. (Color online) (ψ, Δ) spectra obtained from the a-Si:H(392 nm)/SnO_2:F textured structure (open circles) and the results of fitting analyses (solid lines) using (a) model 1, (b) model 2, and (c) model 3 shown in Figs. 2(a), 2(b), and 2(c), respectively.

When the EMA multilayer model in Fig. 2(b) is applied, the fitting improves drastically, particularly at higher energies, as confirmed by Fig. 5(b). As a result, the χ^2 value becomes almost one order of magnitude lower than that of model 1. This shows clearly that the near-surface light reflection in the textured structure can be expressed properly by the EMA multilayer model. In the interference regime at low energies (E < 2.5 eV), however, the calculated spectra show sharp features and the fitting is rather poor, even though the spectral shape is quite similar to the experimental spectra.

The fitting quality in the low energy regime shows a remarkable improvement when the surface area model is adopted, as shown in Fig. 5(c). In this case, the two interference fringes induced by different thicknesses overlap each other, and the sharp interference structure disappears. As a result, the (ψ,Δ) spectra calculated from our model show excellent agreement with the experimental spectra, and the χ^2 value is reduced further by a factor of 10. We find that the area fractions of $A_1 = A_2 = 0.5$ provide quite good fitting. In other words, the two optical models with equal surface area fractions ($A_1 = A_2 = 0.5$) are sufficient to approximate the optical response of the microscopically non-uniform a-Si:H/SnO_2:F textures. Ideally, such non-uniform structures should be represented by multiple optical models with an appropriate distribution of the layer thicknesses. In fact, when the SE analysis was performed using three area fractions of $A_1 = A_2 = 0.33$ and $A_3 = 0.34$, the χ^2 value improved from 4.3 to 3.8. Thus, a more accurate analysis could be achieved if the layer thickness distribution were taken into account, although such attempts have not been made in this study. It should be emphasized that the effect of light scattering on the textured surfaces has been neglected completely in our analysis, because we assumed that the scattered light has different reflection angles and is not detected in the SE measurement. The remarkable agreement between the experimental and calculated spectra confirms that the contribution of the light scattering in the SE measurement is indeed negligible.

The structural parameters and χ^2 obtained from the analyses of Fig. 5 are summarized in Table I. By comparing the results in Table I, it can be seen that values of d_s and d_i obtained from model 1 are underestimated seriously, whereas the d_b value is overestimated. In contrast, the d_{eff} values estimated from models 1-3 are rather similar, as d_{eff} is determined predominantly by the interference pattern at the low energy region.

In order to confirm the SE result in Fig. 5(c), the same sample was measured using transmission electron microscopy (TEM). Figure 6 shows the cross-sectional TEM image of the a-Si:H/SnO_2:F textured structure. The white and black lines in the figure represent the thickness of each layer as estimated from the SE analysis using model 3, and they correspond to the thicknesses of the A_1 region in Fig. 2(c). As confirmed by Fig. 6, the SE result shows remarkable

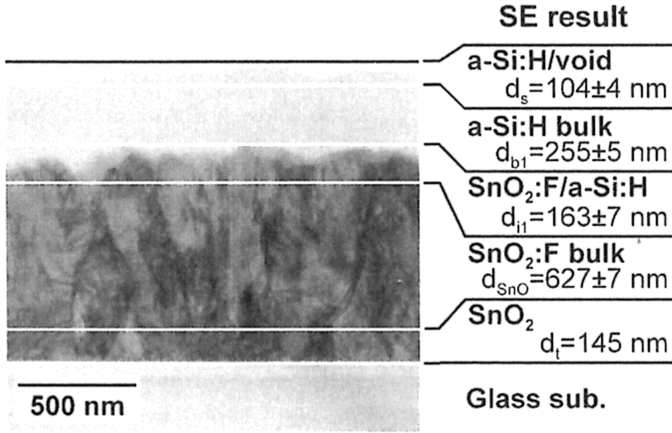

FIG. 6. Cross-sectional TEM image of the a-Si:H/SnO_2:F/glass structure. The white and black lines represent the thicknesses obtained from the SE analysis using model 3 and correspond to the thicknesses of the A_1 region in Fig. 2(c).

agreement with the actual structure. In Fig. 6, however, the structure of the A_2 region is not evident. The A_2 region basically represents the thinner a-Si:H-layer region in the non-uniform a-Si:H/SnO_2:F texture, and it is probable that the wide distribution of the thin layer thicknesses is approximated by the structure of the A_2 region. Thus, we suggest that the structure of the A_2 region is rather hypothetical and is quite difficult to confirm in the actual TEM image.

The results presented above show clearly that the a-Si:H/SnO_2:F textured structure is expressed almost perfectly by combining the surface area and EMA multilayer models, and the analysis method enables the quantitative and high-precision characterization of the textured structure. As mentioned in Sec. III B, the SE analysis has been performed by using the a-Si:H dielectric function obtained from the flat substrate, assuming that the optical constants of the a-Si:H layer are independent of the substrate morphology. Accordingly, the remarkable agreement between the TEM and SE results in Fig. 6 also shows that the optical properties of the a-Si:H layer are basically unaffected by the underlying structure.

B. Effect of a-Si:H layer thickness

In order to determine the variation of the a-Si:H/SnO_2:F textured structure with the a-Si:H layer thickness, a series of a-Si:H layers having different d_{eff} were prepared on the textured SnO_2:F using identical growth conditions. All the a-Si:H/SnO_2:F structures were then characterized by SE analysis using model 3 shown in Fig. 2(c).

Figure 7 shows the (ψ, Δ) spectra obtained from the a-Si:H/SnO_2:F textured structures with (a) $d_{eff} = 125$ nm and

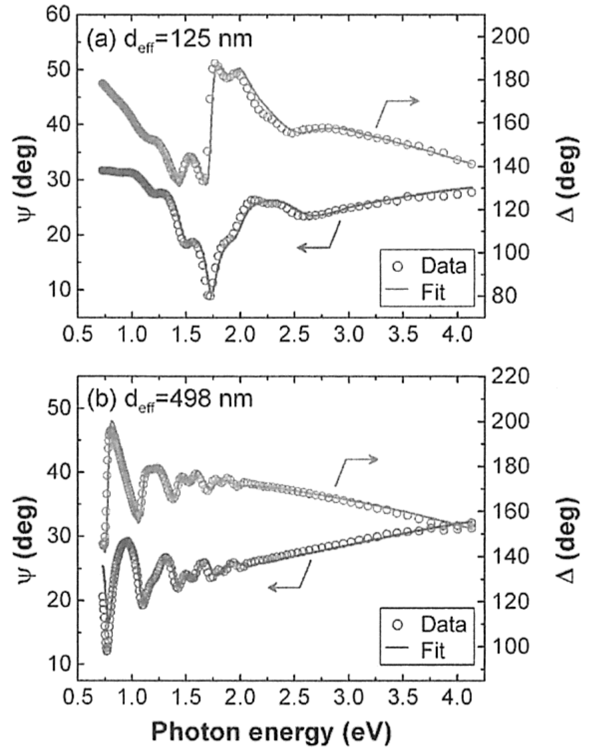

FIG. 7. (Color online) (ψ, Δ) spectra obtained from the a-Si:H/SnO_2:F textured structures with different a-Si:H effective thicknesses of (a) $d_{eff} = 125$ nm and $d_{eff} = 498$ nm. The open circles represent the experimental data, and the solid lines represent the fitting results calculated from model 3.

(b) $d_{eff} = 498$ nm. It can be seen from Fig. 7 that the calculated spectra obtained from the SE analysis show quite good agreement with the experimental data, regardless of the value of d_{eff}. When $d_{eff} = 125$ nm, the complicated interference structure appears in a wide spectral range, as the a-Si:H layer thickness is thin. At $d_{eff} = 498$ nm, however, the interference fringe is confined at $E < 2.2$ eV, and the period of the fringe becomes smaller. In both cases, the fine structure in the (ψ, Δ) spectra is almost completely reproduced in the calculated spectra, supporting the validity of the analysis using model 3.

In order to investigate the a-Si:H layer structure on the SnO_2:F texture, we estimated the d_{eff} of various a-Si:H layers with different thicknesses and compared d_{eff} with the a-Si:H layer thickness obtained using a flat c-Si substrate covered with native oxide (d_{flat}). Figure 8 shows the d_{eff} deduced from the analyses of the a-Si:H/SnO_2:F textured structures, plotted as a function of d_{flat}. The result in Fig. 8 was obtained by using identical deposition times for both substrates. In the a-Si:H deposition on the flat SiO_2/c-Si substrate, the steady-state growth of the a-Si:H occurs at > 50 nm and the a-Si:H thickness increases linearly with the deposition time.[18] From

TABLE I. Structural parameters and biased estimator χ^2 extracted from the SE analyses of the a-Si:H/SnO_2:F textured structures using models 1-3 in Fig. 2. In the SE analyses, a fixed value of $d_t = 145$ nm was employed.

	d_{eff} (nm)	d_s (nm)	α_s	β_s	d_b (nm)	d_i (nm)	α_i	d_{SnO} (nm)	χ^2
Model 1	416 ± 2	18 ± 1			368 ± 1	77 ± 2		788 ± 13	305.5
Model 2	393 ± 32	102 ± 13	5.5 ± 0.9	0.42 ± 0.04	250 ± 11	154 ± 4	3.2 ± 0.2	626 ± 9	36.7
Model 3	392 ± 13	104 ± 4	4.5 ± 0.3	0.41 ± 0.01	255 ± 5 (d_{b1})	163 ± 7 (d_{i1})	3.0 ± 0.1	627 ± 7	4.3
					238 ± 5 (d_{b2})	130 ± 5 (d_{i2})			

Fig. 8, we find that d_{eff} is slightly thicker than d_{flat} and is expressed by $d_{eff} = 1.05d_{flat} + 18$ nm. This result indicates that the deposition rate increases by 5% on the SnO_2:F textured structure, probably due to the slightly higher sticking coefficient of the SiH_3 precursor on the textured structure. The formation of the 18 nm offset in Fig. 8 also suggests that the a-Si:H deposition rate is faster during the initial growth process, although the detail is not clear at this stage.

Figure 9 summarizes the structural parameters of model 3 extracted from the SE analysis of the a-Si:H/SnO_2:F structures, plotted as a function of d_{eff}. In the SE analysis, d_t in Fig. 2(c) showed a constant value of ~150 nm. The TEM result shown in Fig. 6 corresponds to the SE analysis of $d_{eff} = 392$ nm in Fig. 9. The solid lines in the figure show the linear fits to the experimental data, and the equations obtained from the fitting are shown in each panel. The dotted lines in Fig. 9 represent constant values obtained from the analysis. With respect to the surface roughness parameters (d_s, α_s, β_s), α_s and β_s vary linearly with d_{eff}, whereas d_s shows a constant value of 102 nm.

As confirmed by Fig. 9(d), d_{b1} increases quite linearly with d_{eff}. The relation between d_{b1} and d_{eff} is given by $d_{b1} = 0.9d_{eff} - 111$ nm, and thus $d_{b1} = 0$ nm when $d_{eff} \sim 123$ nm. This simply shows the fact that there is no a-Si:H bulk layer when the a-Si:H layer on the texture is quite thin ($d_{eff} < 123$ nm). This can be confirmed from the optical model illustrated in Fig. 2(c) and the TEM image in Fig. 6. Quite interestingly, the thickness ratio of d_{b2}/d_{b1} shows a constant value of 0.9 versus d_{eff}.

The structural parameters for the a-Si:H/SnO_2:F interface (d_{i1}, d_{i2}, α_i) show rather complicated variations with d_{eff}. It can be seen that d_{i1} is constant and the thickness ratio d_{i2}/d_{i1} increases linearly up to ~1 with increasing d_{eff}. This result implies that the sensitivity for the a-Si:H/SnO_2:F interface structure gradually decreases, and we obtain $d_{i1} \sim d_{i2}$ when the a-Si:H is thick enough. As shown in Fig. 9(h), the variation of α_i with d_{eff} comprises the two regions. When $d_{eff} < 228$ nm, α_i shows a large variation, whereas α_i shows a rather constant value at $d_{eff} \geq 228$ nm.

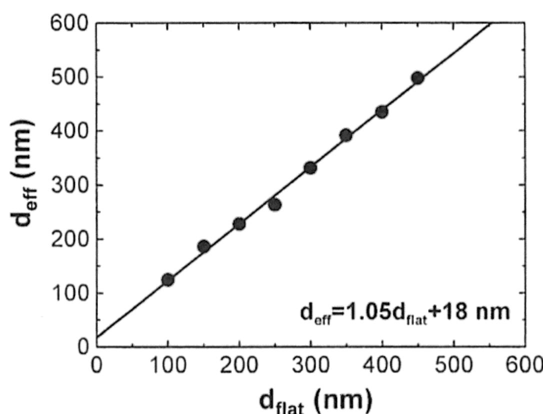

FIG. 8. Effective thickness of the a-Si:H layer in the a-Si:H/SnO_2:F textured structures (d_{eff}), plotted as a function of the a-Si:H layer thickness formed on the flat SiO_2/c-Si substrate using identical growth conditions (d_{flat}). The solid line in the figure represents the fitting result expressed by $d_{eff} = 1.05d_{flat} + 18$ nm.

We found that the large change in α_i at $d_{eff} < 228$ nm is caused by the presence of the void component in the interface region. In particular, when the a-Si:H thickness on the SnO_2:F texture is quite thin, the void component is introduced into the interface layer and the analysis becomes difficult, as model 3 assumes the a-Si:H/SnO_2:F two-phase mixture. On the other hand, the rapid increase in α_i at $d_{eff} < 228$ nm implies an increase in the SnO_2:F fraction in the interface layer. As confirmed by Fig. 4, the refractive index of SnO_2:F ($n = \sqrt{\varepsilon_1} \sim 2$) is much lower than that of a-

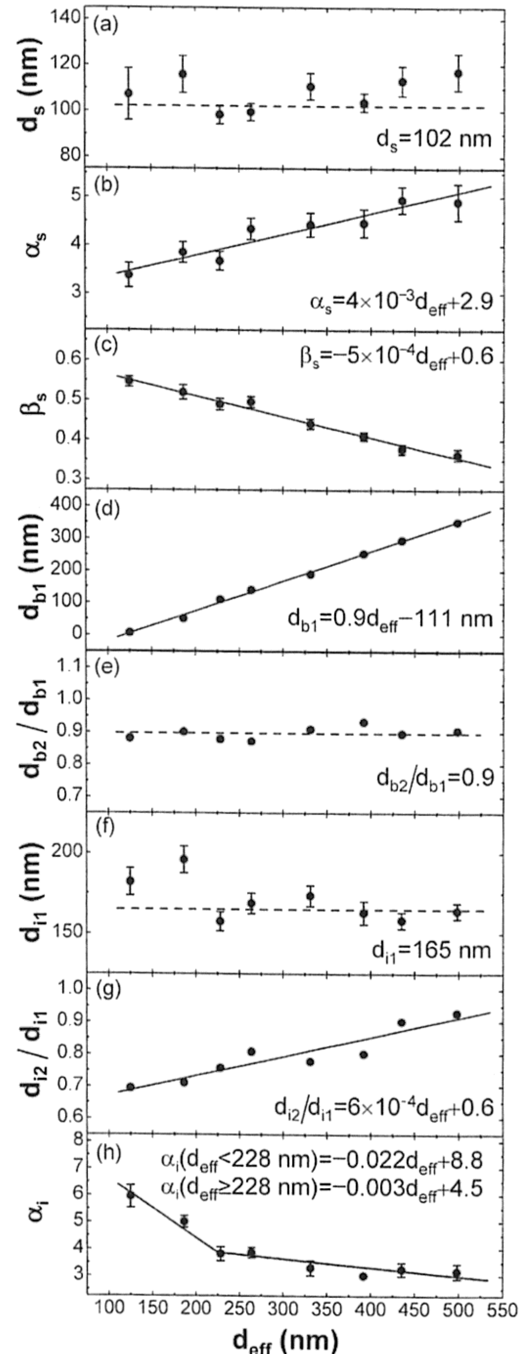

FIG. 9. Structural parameters extracted from the SE analysis of the a-Si:H/SnO_2:F textured structures using model 3, plotted as a function of d_{eff}: (a) d_s, (b) α_s, (c) β_s, (d) d_{b1}, (e) d_{b2}/d_{b1}, (f) d_{i1}, (g) d_{i2}/d_{i1}, and (h) α_i. These parameters represent those indicated in Fig. 2(c). The solid lines show the results of the linear fits, and the corresponding equations are shown in each panel.

Si:H ($n \sim 3.5$). In the analysis of Fig. 9, therefore, when the void component ($n = 1$) is present in the interface region, this effect is compensated by the increase in the SnO_2:F fraction that has the lower refractive index. Thus, the increase in α_i at $d_{eff} < 228$ nm is an artifact, and a three-phase mixture (a-Si:H/SnO_2:F/void) should be assumed in order to perform an accurate analysis of the interface layer when d_{eff} is small. It should be noted that the presence of the void structure in the interface region has been confirmed from the cross-sectional SEM measurements.

In the fitting analysis of Fig. 9, the structural parameters show rather strong correlations. In the case of the surface roughness parameters (d_s, α_s, β_s), for example, the intentional increase in α_s leads to an increase in d_s and β_s values. This can be interpreted by the change in f_{void} in the surface roughness layer. Specifically, the increase in α_s leads to a reduction in f_{void} (or an increase in $f_{a\text{-}Si:H}$) in the surface roughness layer. In the analysis, however, the reduction in f_{void} is compensated by the increase in (d_s, β_s); in other words, the three parameters show correlations, so that the total f_{void} in the surface roughness layer is maintained.

For the variation of the a-Si:H bulk layer, there are also clear correlations between the parameters. For example, the intentional increase in d_{b1} leads to a decrease in d_s and α_s. This simply implies that in order to compensate for the increase in d_{b1}, the thickness as well as the total $f_{a\text{-}Si:H}$ of the surface roughness layer decrease. Quite interestingly, even in this case, we find $d_{b2}/d_{b1} = 0.9$. When the parameters of the interface layer (d_{i1}, d_{i2}, α_i) are varied intentionally, all the other parameters change, and the interpretation of the parameter correlations becomes more difficult.

It is evident from Fig. 9 that the SE analysis can be performed by fixing three parameters (d_s, d_{b2}, d_{i1}). If the value of d_t is fixed, the number of fitting parameters decreases from nine to six (α_s, β_s, d_{b1}, d_{i2}, α_i, d_{SnO}). Moreover, if we employ the equations shown in Fig. 9, the fitting can be carried out using only one parameter, d_{eff}, assuming that the a-Si:H layer structure on the SnO_2:F texture is universal and is controlled only by d_{eff}.

With the result of Fig. 9, we further investigated the surface roughness evolution with d_{eff}. Figure 10 shows the variation of $f_{a\text{-}Si:H}$ and f_{void} in the surface roughness layer for $d_{eff} = 125$ nm, 331 nm, and 498 nm. The results of Fig. 10 were calculated from the EMA multilayer model using the parameter values of d_s, α_s, and β_s shown in Fig. 9. As mentioned earlier, with increasing d_{eff}, α_s increases whereas β_s decreases. It can be seen from Fig. 10 that these changes in α_s and β_s correspond to the filling of the a-Si:H component in the cylinder geometry illustrated in Fig. 3. Accordingly, the SE result in Fig. 9 shows that the cross-sectional structure of the a-Si:H roughness changes from a round shape to a trapezoidal shape with increasing d_{eff}.

In order to confirm the surface roughness evolution shown in Fig. 10, the surface structures of the a-Si:H/SnO_2:F samples were measured by atomic force microcopy (AFM). Figure 11 shows the AFM images of the a-Si:H/SnO_2:F textured structures for (a) $d_{eff} = 125$ nm, (b) $d_{eff} = 228$ nm, (c) $d_{eff} = 331$ nm, and (d) $d_{eff} = 498$ nm. In the figure, the values of the root-mean-square roughness (d_{rms}) obtained from

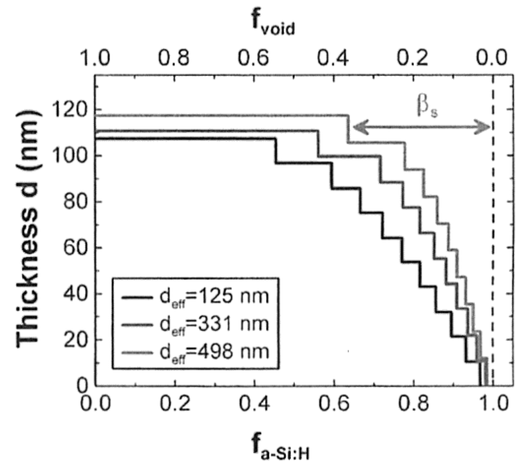

FIG. 10. (Color online) Variation of $f_{a\text{-}Si:H}$ and f_{void} for the thickness d in the surface roughness layer incorporated in model 3. These lines are calculated from the d_s, α_s, and β_s values for each d_{eff} in Fig. 9. Note that $f_{void} = 1 - f_{a\text{-}Si:H}$.

AFM images with a scan size of 2×2 μm^2 are shown, together with d_s determined from the SE analyses. The AFM images reveal that the surface shape becomes rounder and the void fraction decreases with increasing d_{eff}. Thus, the AFM result in Fig. 11 is basically consistent with the SE result shown in Fig. 10. In the SE measurements of the texture surfaces, however, only specular light reflection is measured, and the light scattered by the surface texture is not detected. Accordingly, the correlation between the AFM and SE results is rather qualitative at this stage. From Fig. 11, we find that d_{rms} decreases gradually with increasing d_{eff}, whereas d_s is rather constant. For a better understanding of the a-Si:H surface structure, such SE and AFM results should be investigated further.

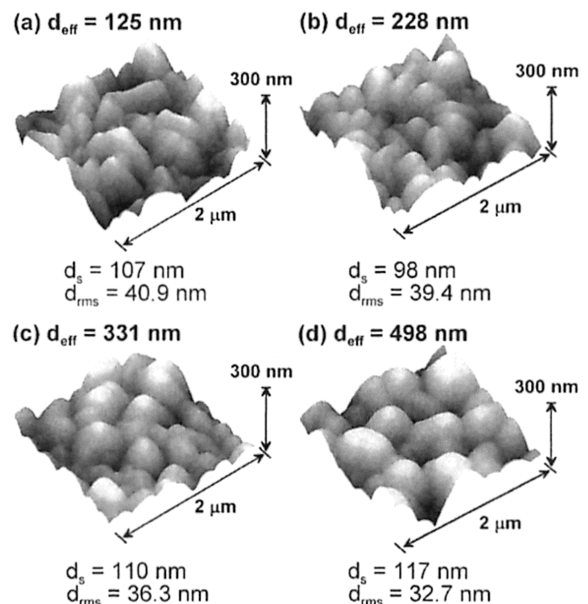

FIG. 11. (Color online) AFM images of the a-Si:H layers formed on the SnO_2:F texture with (a) $d_{eff} = 125$ nm, (b) $d_{eff} = 228$ nm, (c) $d_{eff} = 331$ nm, and (d) $d_{eff} = 498$ nm. The d_s and d_{rms} in each panel denote the surface roughness layer thickness determined by SE and the root-mean-square roughness obtained by AFM, respectively.

V. CONCLUSION

We have established a SE analysis method that can be applied for the high-precision structural analysis of a-Si:H/ SnO_2:F textured structures. In order to express the optical response in the a-Si:H surface roughness and a-Si:H/SnO_2:F interface regions accurately, we have developed an EMA multilayer model in which a two-phase multilayer structure is assumed in a cylindrical geometry. Moreover, to model the microscopic structural inhomogeneity of the a-Si:H/ SnO_2:F texture, we further applied a surface area model that employs two optical models with different layer thicknesses. By applying an optical model that incorporates the EMA multilayer and surface area models, the ellipsometry spectra obtained from the a-Si:H/SnO_2:F structures are almost perfectly reproduced, and the structure determined by TEM shows excellent agreement with that deduced from the SE analysis, supporting the validity of our analysis. From the above results, we find that (i) the effect of light scattering can be neglected in the SE analysis, as the contribution of the scattered light in the SE measurement is quite small, and (ii) the optical properties of the a-Si:H layer are basically unaffected by the underlying SnO_2:F textures. The optical model developed in this study provides excellent fitting to various a-Si:H/SnO_2:F structures with different a-Si:H layer thicknesses, and we have expressed the structural parameters as a function of the a-Si:H layer thickness. If we utilize these values, the SE analysis is carried out by using only one parameter for the a-Si:H thickness. The above results show clearly that our SE analysis method is quite effective in characterizing a-Si:H/SnO_2:F textured structures. Finally, we note that the SE technique provides a new promising way of determining the detailed layered structures in large-area a-Si:H modules.

[1]C. Beneking, B. Rech, S. Wieder, O. Kluth, H. Wagner, W. Frammelsberger, R. Geyer, P. Lechner, H. Rübel, and H. Schade, Thin Solid Films **351**, 241 (1999).

[2]Y. Tawada, H. Yamagishi, and K. Yamamoto, Sol. Eng. Mater. Sol. Cells **78**, 647 (2003).

[3]G. P. Willeke, Sol. Eng. Mater. Sol. Cells **72**, 191 (2002).

[4]H. Fujiwara, *Spectroscopic Ellipsometry: Principles and Applications* (Wiley, West Sussex, England, 2007).

[5]P. I. Rovira and R. W. Collins, J. Appl. Phys. **85**, 2015 (1999).

[6]P. I. Rovira, A. S. Ferlauto, J. Koh, C. R. Wronski, and R. W. Collins, J. Non-Cryst. Solids **266–269**, 279 (2000).

[7]M. Mizuhashi, Y. Gotoh, and K. Adachi, Jpn. J. Appl. Phys. **27**, 2053 (1988).

[8]T. Ikeda, K. Sato, Y. Hayashi, Y. Wakayama, K. Adachi, and H. Nishimura, Sol. Eng. Mater. Sol. Cells **34**, 379 (1994).

[9]S. Kageyama, M. Akagawa, and H. Fujiwara, Phys. Rev. B **83**, 195205 (2011).

[10]R. H. Muller and J. C. Farmer, Surf. Sci. **135**, 521 (1983).

[11]H. L. Maynard, N. Layadi, and J. T. C. Lee, Thin Solid Films **313–314**, 398 (1998).

[12]S.-J. Cho, P. G. Snyder, C. M. Herzinger, and B. Johs, J. Vac. Sci. Technol. B **20**, 197 (2002).

[13]G. E. Jellison, Jr., Appl. Opt. **30**, 3354 (1991).

[14]G. E. Jellison, Jr., Thin Solid Films 290–291, 40 (1996).

[15]C. M. Herzinger, B. Johs, W. A. McGahan, J. A. Woollam, and W. Paulson, J. Appl. Phys. **83**, 3323 (1998).

[16]G. E. Jellison, Jr., and F. A. Modine, Appl. Phys. Lett. **69**, 371 (1996); **69**, 2137 (1996).

[17]H. Fujiwara and M. Kondo, Phys. Rev. B **71**, 075109 (2005).

[18]H. Fujiwara, M. Kondo, and A. Matsuda, J. Appl. Phys. **91**, 4181 (2002).